

pubs.acs.org/Macromolecules Article

Phenazine-Substituted Poly(benzimidazobenzophenanthrolinedione): Electronic Structure, Thin Film Morphology, Electron Transport, and Mechanical Properties of an n-Type Semiconducting Ladder Polymer

Sarah M. West, Duyen K. Tran, Jiajie Guo, Shinya E. Chen, David S. Ginger, and Samson A. Jenekhe*



Cite This: https://doi.org/10.1021/acs.macromol.2c01999



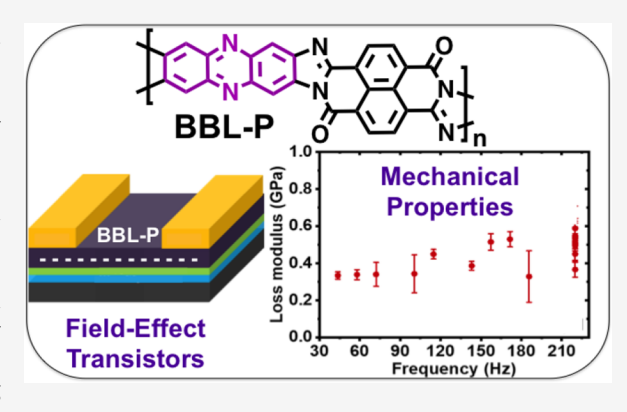
ACCESS

III Metrics & More

Article Recommendations

s Supporting Information

ABSTRACT: Unlike naphthalene diimides, perylene diimides, and other classes of n-type conjugated polymers with numerous derivatives that enable understanding of structure—property relationships, the electronic structure and properties have not been reported for any derivative of ladder poly(benzimidazobenzophenanthroline) (BBL). Herein, we report the synthesis and properties of BBL-P, a phenazine derivative of BBL. In acid solution, BBL-P has a broad absorption spectrum with a lowest energy absorption peak at 840 nm due to protonation-enhanced intramolecular charge transfer. Compared to BBL, BBL-P thin films have decreased crystallinity with face-on molecular orientations on substrates, resulting in a substantially decreased field-effect electron mobility of $1.2 \times 10^{-4}~\text{cm}^2/\text{V}$ s. BBL-P films have excellent mechanical properties exemplified by a Young modulus of 11 GPa. The results demonstrate that BBL-P is a promising



n-type semiconducting polymer and provide new insights into the effects of backbone structure on electronic structure, thin film microstructure, and charge transport properties of conjugated ladder polymers.

INTRODUCTION

By virtue of their double-stranded or all-polycyclic architectures, π -conjugated ladder polymers have an ideal persistent ribbon-like conformation that is free of torsional disorders. They are thus promising for applications in organic electronics and optoelectronics as well as for basic understanding of structure—property relationships in semiconducting polymers. Among the most widely studied π -conjugated ladder polymers is the prototype n-type semiconducting polymer, ladder poly(benzimidazobenzophenanthroline) (BBL) (Chart 1). Although first synthesized in 1966 by van Deusen, more than a decade before the discovery of doped conducting polymers in 1977, the early chemical, electrochemical, and ion-implantation doping methods BBL to the highly conducting state were reported in the 1980s. Our group

Chart 1. Molecular Structures of π -Conjugated Ladder Polymers BBL and BBL-P

reported the n-type semiconducting charge transport properties of BBL in 2002, 8-10 leading to the demonstration of this ladder polymer as the first conjugated polymer-based high-performance, n-channel field-effect transistors (OFETs). 11 The n-type semiconducting properties of BBL have since been extensively investigated and successfully used in various device applications including organic photovoltaics (OPVs), 12,13 organic electrochemical transistors (OECTs), 14-16 organic field-effect transistors (OFETs), 8,17-19 organic thermoelectrics, 20-22 and supercapacitors. 23 Recently, ground-state charge transfer between neutral BBL and a neutral polythiophene derivative was observed, resulting in highly conducting polymer blend films without external doping. 24 However, unlike other classes of n-type conjugated polymers such as perylene diimides, 25,26 naphthalene diimides, 27,28 and other arylene diimides, with numerous derivatives that enable understanding of structure—property relationships, very few

Received: September 28, 2022 Revised: February 13, 2023



derivatives of BBL have been reported.^{33–37} Furthermore, very little is known about the electronic structure and properties of the few known BBL derivatives.

One intriguing derivative of BBL is the phenazine-substituted ladder polymer BBL-P, whose molecular structure is shown in Chart 1. Its synthesis was reported in 1974 in the context of thermally stable polymers for aerospace applications. However, the electronic structure, field-effect charge transport, and other physical properties of BBL-P have not been reported heretofore. Phenazine as a molecular building block has appealing features. The reduction potential of phenazine ($E_{1/2} = -1.19$ V vs SCE) is over 2 V more positive than benzene ($E_{1/2} = -3.42$ V vs SCE), ^{38,39} which suggests that its incorporation into conjugated polymers may enable achievement of high electron affinity and thus potential as n-type semiconducting polymers. Many p-type semiconducting polymers with donor—acceptor (D-A) architectures have incorporated a phenazine-1,4-diyl (1,4-phen) unit (Chart 2)

Chart 2. Different Linkage Positions for Incorporating Phenazine (phen) into π -Conjugated Polymer Backbones

as the acceptor moiety with donor moieties such as indacenodithienothiophene, 40 indacenodithiophene, 41,42 benzodithiophene, $^{43-47}$ fluorene, 48 carbazole, $^{49-51}$ and dithienopyrrole. 52 These 1,4-phen-containing D-A copolymers have typical optical bandgaps of about 1.5–2.4 eV and space-charge limited current (SCLC) hole mobilities of 10^{-2} to 10^{-5} cm $^2/V$ s, which have enabled their applications in polymer solar cells. π -Conjugated poly(phenazine-2,7-diyl) bearing 1,2,5,8-tetraalkyl side chains and two derivatives have been synthesized and shown to have high electron affinity (\sim 4.1 eV) from cyclic voltammetry experiments, and thus they were suggested to be n-type semiconducting polymers; however, electrical conductivity or charge transport properties were not reported for any of these polymers.

Here, we report the synthesis and investigation of the electronic structure, thin film microstructure, and optical, electron transport, and mechanical properties of the conjugated ladder polymer, poly[7-oxo-7H,12H-benz[4',5']isoquino [2',1':1,2] imidazo [4,5-b] imidazo [4,5-i] phenazine-3,4:12.13-tetrayl)-12-carbonyl] (BBL-P). Although a moderate molecular weight was indicated by the measured intrinsic viscosity ($[\eta]$) (0.68 dL/g in methanesulfonic acid (MSA) and 1.1 dL/g in conc. H_2SO_4 at 30 °C), the BBL-P sample could form strong and flexible freestanding films. The molecular structure of BBL-P was confirmed by elemental analysis and FTIR and Raman spectroscopic techniques. Unlike BBL, which exhibits a relatively narrow absorption spectrum in MSA solution, we found that BBL-P has an unusually broad absorption spectrum in MSA solution with a lowest energy absorption peak at 840 nm due to protonation-enhanced intramolecular charge transfer (ICT). We characterized the mechanical properties of BBL-P films and found the Young modulus to be 11 GPa. BBL-P thin films have an optical

bandgap of 1.6 eV, cyclic voltammetry derived LUMO energy level of -4.0 eV, and HOMO energy level of -5.5 eV. As the n-channel material in organic field-effect transistors (OFETs), BBL-P showed an average electron mobility of $\sim\!1.0\times10^{-4}$ cm²/V s. Our BBL-P results contribute important insights for the design of new high-performance BBL derivatives. We believe that BBL-P will be an attractive n-type semiconducting polymer for various organic electronic applications including thermoelectric and OECT. In particular for OECT, n-type materials are rare, $^{16,54-56}_{16,54-56}$ with the performance lagging behind p-type materials. $^{57-59}$

EXPERIMENTAL METHODS

Materials and Methods. The monomer 1,4,5,8-naphthalenete-tracarboxylic acid was purchased from TCI and purified according to a modified procedure. On 2,3,7,8-Tetraaminophenazine hydrochloride was synthesized according to the published procedures. Sodium acetate, polyphosphoric acid (PPA, 84% P₂O₅), phosphorus pentoxide, and methanesulfonic acid (MSA) (>99%) were purchased from Sigma-Aldrich and used as received. Methanol and concentrated sulfuric acid were purchased from Fisher Scientific and used as received.

Intrinsic viscosity of BBL-P in both MSA and H_2SO_4 was measured by an Ubbelohde viscometer suspended in a water bath at 30.0 °C. The concentrations of the polymer solutions were chosen such that the elution time of the polymer solution was 1.1–1.8 times that of the pure solvent. Thermogravimetric analysis (TGA) was conducted on a TA Instrument model Q50 TGA. A heating rate of 10 °C/min under a flow of N_2 was used with runs conducted from room temperature to 880 °C. Differential scanning calorimetry (DSC) analysis was performed on a TA Discovery DSC 500 under N_2 by scanning from –10 to 400 °C at a heating rate and cooling rate of 10 °C/min. The 1H NMR spectrum was recorded on a Bruker AV500 (at 500 MHz) using deuterated nitromethane/GaCl $_3$ as the solvent. Optical absorption spectra were measured on a PerkinElmer model Lambda 900 UV–vis/near-IR spectrophotometer. Solution absorption spectra were obtained from dilute (10^{-5} M) solutions in MSA.

Cyclic voltammetry (CV) experiments were done on an EG&G Princeton Applied Research potentiostat/galvanostat (model 273A). A three-electrode cell was used, using a platinum wire as the counterelectrode and BBL-P spin-coated onto indium tin oxide (ITO) substrates as the working electrode. The reference electrode was Ag/AgNO3 in acetonitrile. The BBL-P working electrode was fabricated by coating BBL-P solution in MSA onto ITO substrates. The acidic solvent was removed by dipping the substrate in isopropanol (IPA) overnight and was subsequently dried in a vacuum oven at 60 °C. The supporting electrolyte solution consists of 0.1 M tetrabutylammonium hexafluorophosphate (Bu₄NPF₆) in anhydrous acetonitrile. The electrolyte was purged with nitrogen for 15 min prior to the CV scans to ensure anerobic and anhydrous conditions. The reduction and oxidation potentials were referenced to the Fc/Fc+ couple by using ferrocene as an internal standard. The LUMO energy level was estimated using a ferrocene value of -4.8 eV with respect to the vacuum level. The LUMO and HOMO levels were determined by using the equations $E_{\text{LUMO}} = -(eE_{\text{red}}^{\text{onset}} + 4.8)$ and $E_{\text{HOMO}} = -(eE_{\text{ox}}^{\text{onset}} + 4.8)$.

Fourier-transform infrared (FTIR) spectroscopy experiments were performed on a Perkin Elmer Frontier spectrometer by using BBL-P freestanding films. The resolution was set at 1 cm⁻¹ and a set of 16 scans was averaged. Raman spectroscopy of BBL-P freestanding films was carried out on a Thermo Scientific DXR2 Raman microscope. A 532-nm laser with a power of 5 mW was focused onto a sample through a 50× objective lens.

Atomic force microscopy (AFM) characterization of the surface morphology of the BBL-P films was done using a Bruker Dimension scanning probe microscope (SPM) system. Films of BBL-P were prepared as described earlier. Grazing incidence wide-angle X-ray scattering (GIWAXS) measurements were conducted at the Advanced

Scheme 1. Synthesis of BBL-P (PPA = Polyphosphoric Acid, 84% Free P₂O₅)

Light Source (ALS) at the Lawrence Berkley National Laboratory by using the beamlines 7.3.3 and a Pilatus 2 M area detector. The images were taken with a beam energy of 10 keV and incidence angle 0.14° with 5 s exposure time. Data were processed using Nika and WAXStools in Igor Pro. Peak positions were determined by Lorentzian peak fittings. The crystal coherence length (L_c) of samples was determined by using the Scherrer equation: $L_c = 2\pi K/\Delta q$, where K is a shape factor (typically 0.9) and $L_c = 2\pi K/\Delta q$, where $L_c = 2\pi K/\Delta q$ is the full width at the $L_c = 2\pi K/\Delta q$, where $L_c = 2\pi K/\Delta q$ is the full width at the $L_c = 2\pi K/\Delta q$, where $L_c = 2\pi K/\Delta q$ is the full width at the $L_c = 2\pi K/\Delta q$ is the full width at the $L_c = 2\pi K/\Delta q$ is the full

Gas-phase molecule density functional theory (DFT) calculations were performed using the Gaussian 16 suite of programs 63 at the ω B97XD/631-G(d,p) level of theory on the representative oligomer comprising three repeat units oriented in a *trans-cis-trans* geometry to represent the polymer backbone.

Synthesis of BBL-P. PPA (20.64 g) was added to a reaction vessel equipped with a mechanical stirrer and heated to 150 °C and purged with nitrogen overnight. The PPA was cooled to 40 °C, and 2,3,7,8tetraaminophenazine HCl (1.606 g, 5.4 mmol) was added. The temperature was increased to 75 °C and stirred for 4 h under dynamic vacuum. The temperature was then reduced to 65 °C and 1,4,5,8naphthalenetetracarboxylic acid (1.656 g, 5.4 mmol) was added. The mixture was stirred for 45 min before P₂O₅ (3.090 g, 21.8 mmol) was added portionwise. The temperature was increased to 100 °C and stirred overnight. The temperature was then slowly increased to 150 °C and stirred for 24 h. The temperature was further increased to 180 °C and stirred for 3 days. The reaction mixture was cooled to room temperature, and water was added to quench the reaction. The polymer mass was added to a blender, cut into pieces, and washed with water by Soxhlet extraction for 3 days. The crude polymer was then added to 4 L of water, boiled for 24 h, and dried under vacuum. The crude polymer was further purified by reprecipitation from H₂SO₄ into 1:1 water/methanol and thoroughly dried at 200 °C under vacuum (2.212 g, 82%). Intrinsic viscosity $[\eta]$: 1.1 dL/g (30.0 °C, conc. Sulfuric acid). Anal. calcd for $C_{26}H_{14}N_6O_5$ (%) (BBL-P powder): C, 63.67; H, 2.88; N, 17.14; O, 16.31; found (%): C, 58.56; H, 3.21; N, 17.20; O, 16.17. Anal. calcd for C₂₆H₁₂N₆O₄ (%) (BBL-P freestanding film): C, 66.10; H, 2.56; N, 17.79; O, 13.55; found (%): C, 63.39; H, 2.47; N, 18.74; O, 13.04.

Fabrication and Characterization of OFETs. n-Channel organic field-effect transistors (OFETs) were fabricated in a bottom-gate/top-contact device architecture with a polymer buffer layer. The substrate comprises heavily n-doped silicon (<0.005 S/cm; $500 \mu m$) with a 300 nm-thick silicon oxide layer. The substrates were cleaned by sequentially sonicating in DI water, acetone, and isopropyl alcohol. The cleaned substrates were then treated with air plasma for 10 min. Insulating polystyrene (PS) was dissolved in anhydrous toluene (5 mg/mL) and stirred at room temperature overnight. The PS solution was spin-coated onto the substrates at 3000 rpm for 60 s followed by drying in a vacuum oven at 60 °C overnight to produce a 17.0 nm (\pm 0.12 nm) thick layer. On top of the PS-coated substrates, the BBL-P thin films were deposited by spin-coating a BBL-P solution in MSA (25 mg/mL) at 5000 rpm for 30 s. The acidic solvent was removed by dipping the films in a mixture of isopropanol (IPA) and ethylene glycol (EG) (1:1, v:v) several times for 12 h. Afterward, the BBL-P films were submerged in 100% IPA for at least 5 h to wash away excess ethylene glycol. Finally, the BBL-P films were dried in a vacuum oven at 100 °C overnight and then annealed at 170 °C on a hot plate for 10 min in a nitrogen-filled glovebox. Source and drain electrodes were defined by thermal evaporation of gold electrodes (60

nm). Channel width (W) and length (L) were 1000 μ m and 100 μ m, respectively. The transistors were tested by using a Keithley 4200 semiconductor characterization system inside a nitrogen atmosphere. The field-effect electron mobility (μ) was extracted by analyzing the current–voltage data with the saturation-region equation:

$$I_{\rm ds} = \frac{\mu W C_{\rm i}}{2L} (V_{\rm gs} - V_{\rm t})^2$$

where $I_{\rm ds}$ is the source-drain current, μ is the field-effect mobility, $C_{\rm i}$ is the capacitance of gate insulator (10.6 nF/cm²), $V_{\rm gs}$ is the source-gate voltage bias, and $V_{\rm t}$ is the threshold voltage.

Characterization of Mechanical Properties by the Nanoindentation Test. The elastic modulus was measured using a Hysitron TI 980 TriboIndenter. The nanoindentation test required a Berkovich tip compressing into the sample while measuring the force and displacement. The tests were carried out in both constant displacement and constant load mode. Three indents were made across the film surface at each displacement and load value. The reported elastic modulus was the average of the moduli in the range of 10-20% depth into the total film thickness to minimize any substrate effects. Dynamic mechanical analysis (DMA) was done by applying an oscillating load with maximum amplitude of $100~\mu\text{N}$ at varying frequencies from 45 to 200 Hz. Samples were made by spin-coating BBL-P onto a glass substrate using procedure described earlier. The total thickness of the BBL-P sample was determined to be 650 nm using a profilometer.

■ RESULTS AND DISCUSSION

Synthesis and Characterization. The synthetic route to the ladder polymer BBL-P is shown in Scheme 1. The 2,3,7,8tetraaminophenazine hydrochloride monomer was synthesized according to the published procedure, which produced the monomer in high purity.³⁴ The 1,4,5,8-naphthalenetetracarboxylic acid co-monomer, purchased with 60% purity, was rigorously purified according to the published procedure before use. ⁶⁰ A unique characteristic of rigid-rod polymers is that polymerization in the liquid crystalline phase yields higher molecular weights than polymerization in the isotropic phase.⁶⁴ Therefore, we modified the original synthetic procedure in an attempt to induce liquid crystallinity during polymerization. However, we did not observe stir-opalescence or other evidence of liquid crystallinity. When first synthesized in 1974, the isotropic phase condensation in pure polyphosphoric acid (PPA) resulted in BBL-P with low intrinsic viscosity ($[\eta]$) of 1.1 dL/g in methanesulfonic acid (MSA) at 30 °C.3 However, our BBL-P sample also gave a low $[\eta]$ value of 1.1 dL/g in concentrated sulfuric acid (H₂SO₄) at 30 °C, which is nearly identical to that measured in 1974, 34 confirming that our synthesis of BBL-P also took place in the isotropic phase.

The BBL-P sample was isolated as a black solid powder and shows a purple color in either concentrated H_2SO_4 or MSA. In addition to the low $[\eta]$ of BBL-P in concentrated H_2SO_4 (1.1 dL/g) at 30 °C, we found that $[\eta]$ was 0.68 dL/g in MSA at 30 °C. The solvent-dependent viscosity of BBL-P solutions, which is in contrast with the constant $[\eta]$ of BBL regardless of solvent, ⁶⁵ may be due to the improved solubility of BBL-P in H_2SO_4 compared to MSA. The molecular structure of BBL-P was confirmed by elemental analysis and FTIR and Raman

spectroscopic techniques. The analytical data for each element match the calculated values except carbon, which was lower than those calculated mainly due to incomplete combustion, which is a common problem in the elemental analyses of thermally stable polymers. ^{1,60,64,66} Interestingly, the elemental analysis of the BBL-P powder revealed a total of ~11 wt % water was retained, which is equivalent to approximately three water molecules per repeat unit, suggesting that BBL-P is intrinsically hygroscopic in marked contrast from the parent BBL. ⁶⁷ The hygroscopic nature of BBL-P is likely to originate from the phenazine moieties whereby the imine nitrogen sites are free to hydrogen bond with absorbed water molecules from the atmosphere. ⁶⁸

The hygroscopic nature of BBL-P was further corroborated by thermogravimetric analysis (TGA) as shown in Figure S1a. An initial weight loss of ~8.1% was observed at 80-110 °C, which can be attributed to water evaporation. Additional rigorous drying of BBL-P at 200 °C for 48-96 h under vacuum was found to be insufficient to completely remove water. This result supports the elemental analysis that also showed residual water in BBL-P. To get a clear picture of the thermal stability, the TGA scans were performed after drying by first scanning to 200 and 400 °C and then cooling down to 50 °C and heating to 880 °C under nitrogen (Figure S1a). The results show that BBL-P is stable in high temperatures in agreement with similar ladder polymers, 34,69 showing 5% weight loss at 609 °C and 626 °C in an inert atmosphere for samples dried at 200 and 400 °C, respectively. Differential scanning calorimetry (DSC) scans showed no detectable phase transitions in the 25 to 400 °C temperature range (Figure S1b), which agrees with literature reports of the very high glass transition temperature $(T_{\rm g})$ of ladder polymers (>400 °C). 65 The observed excellent thermal stability and high T_g of BBL-P are comparable to those of BBL.⁶⁰ To further characterize the molecular structure of BBL-P, we collected ¹H NMR spectra for both BBL-P-GaCl₃ and BBL-GaCl₃ complexes in deuterated nitromethane⁶⁵ and they are shown in Figure S2a,b. We note that soluble Lewis acid complexes of rigid-rod ladder polymers have allowed the study of both solution and solid-state properties of BBL in the last few several decades. 65,69 Solutions of both polymers were prepared in deuterated nitromethane containing GaCl₃ according to the known procedures. 65 However, the use of Lewis acid complexes to acquire NMR spectra is known to produce multiple impurity peaks for benzimidazobenzophenanthroline polymers; 36,65,69 these impurities appear at \sim 7.3, 8.5, 9.1, and 10.5 ppm for BBL-P (Figure S2a) and BBL (Figure S2b). The broad overlapped resonances of both polymers are due to the presence of 6 possible cis and trans structural isomers¹⁹ and are shown in Figure S2c; these isomers make unambiguous peak assignments difficult. However, comparison of the two spectra does allow assignment of the resonances associated with the co-monomers. The NMR spectra show unresolved peaks from the naphthalene protons at ~9.3-9.8 ppm for BBL-P and ~9.6-9.8 ppm for BBL. The phenazine protons in BBL-P are assigned to the four resonances centered at 7.2, 7.5, 8.6, and 8.9 ppm, whereas the benzene protons for BBL are assigned to the singlet within the naphthalene cluster at 9.8 ppm and the overlapped resonance at 9.0 ppm.^{36,65}

To enable further characterization of the molecular structure, thin film microstructure, and optical properties of BBL-P, we prepared freestanding films. The detailed procedure for the fabrication of BBL-P freestanding films is described in

the Supporting Information. Briefly, the spin-coated BBL-P film on glass substrates was baked at 120 °C overnight on a hot plate in an ambient atmosphere to evaporate most of the acidic solvent. The baked film was slowly cooled down to room temperature and subsequently submerged in water whereby the film swelled significantly due to the intrinsic hygroscopic nature of BBL-P. As a result, BBL-P thin films could be peeled off from the supporting glass substrates and lifted off from water (Figure 1a) to form freestanding films (Figure 1b) with

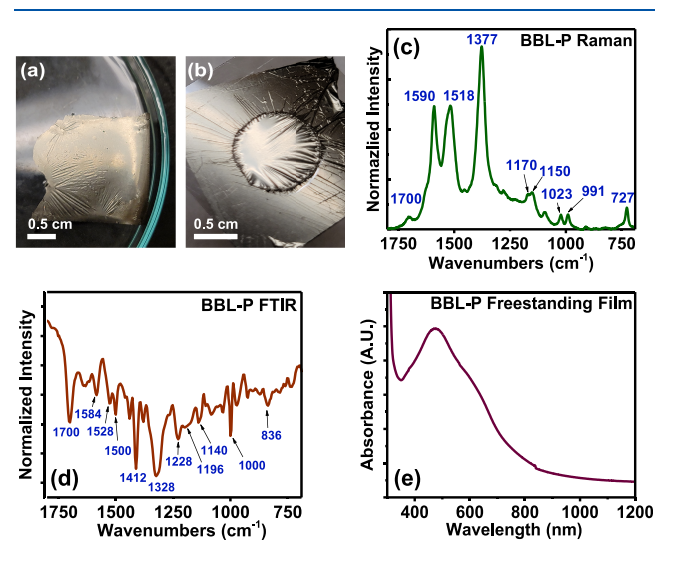


Figure 1. (a) BBL-P film floating on water after peeling off from the initial supporting substrate. (b) Freestanding BBL-P film with a diameter of 1 cm. (c) Raman spectrum of BBL-P freestanding film with an excitation laser of 532 nm. (d) Fourier-transform infrared (FTIR) spectrum of BBL-P freestanding film. (e) Optical absorption spectrum of BBL-P freestanding film.

surface area as large as $5-6~\rm cm^2$. We note that films of larger area can also be fabricated by extending the area of the initial supporting substrates. The freestanding films have good quality and were used to characterize the molecular structure through elemental analysis, UV–Vis optical absorption, Fourier-transform infrared (FTIR), and Raman spectroscopic techniques.

FTIR spectroscopy in conjunction with Raman spectroscopy was used to confirm the molecular structure of BBL-P in addition to the previously discussed elemental analysis. The FTIR and Raman spectra of freestanding BBL-P films collected in an ambient atmosphere are shown in Figure 1c,d. The peak positions assigned to various vibration modes are summarized in Table 1. The prominent $\nu(C=O)$ carbonyl carbon-oxygen stretch mode can be seen on both the FTIR and Raman spectra with distinct absorption peaks at 1700 cm^{-1} (Table 1). The imine carbon-nitrogen stretch mode, $\nu(C=N)$, can be identified by an intense Raman absorption band at 1590 cm⁻¹ and a low intensity FTIR absorption band at 1584 cm⁻¹. At lower wavenumbers, there is an intense Raman absorption band at 1518 cm⁻¹ and some weak-intensity FTIR bands at 1528 and 1500 cm⁻¹, which can be attributed to aromatic carbon-carbon and carbon-nitrogen skeletal vibrations (Table 1).65 Moreover, a sharp and intense FTIR absorption band at 1412 cm⁻¹ can be assigned to carbon-nitrogen amide bonds, 65 ν (C-N), which further supports backbone fusion. Additional FTIR absorption bands at 1380 and 1328 cm⁻¹ coupled with a Raman absorption band at 1377 cm⁻¹ originate

Table 1. FTIR and Raman Absorption Bands of Freestanding BBL-P Film and Their Peak Assignments

FTIR absorption band (cm ⁻¹)	Raman absorption band (cm ⁻¹)	assignment		
1700	1700	ν (C=O), carbonyl carbon–oxygen stretch		
1584	1590	ν (C=N), imine carbon-nitroger stretch		
1528, 1500	1518	aromatic carbon–carbon, carbon– nitrogen skeletal vibrations		
1412		$\nu(\text{C-N})$, carbon—nitrogen amide bonds		
1380, 1328	1377	$\nu(\text{C-N})$, carbon—nitrogen single bonds		
1228, 1000	1023, 991	mixed skeletal vibrations		
	1170, 1150	in-plane C-H bending		
972, 836		out-of-plane C–H wagging		
	727	$\delta(\text{C-H})$, out-of-plane wag of naphthalene C-H bonds		

from the stretching of carbon–nitrogen single bonds, ⁶⁵ ν (C–N), in the BBL-P polymer.

Skeletal vibrations also appeared in both the FTIR and Raman spectra, respectively, at 1228 and 1000 cm⁻¹ and at 1023 and 991 cm⁻¹ (Table 1). 65 In-plane C-H bending can be assigned to absorption bands centered at 1170 and 1150 cm in the Raman spectrum whereas out-of-plane C-H wagging can be seen at 972 and 836 cm⁻¹ in the FTIR spectrum (Table 1). A sharp Raman absorption band at 727 cm⁻¹ can be attributed to the out-of-plane C-H wagging of the two adjacent carbonhydrogen bonds on the naphthalene rings (Table 1). We note that no $\nu(O-H)$ peak was observed in the FTIR spectrum suggesting that the absorbed water seen in the BBL-P powder, which was used in TGA and elemental analysis, had been effectively removed in the BBL-P freestanding film. One possible explanation for the lack of observed water in the FTIR spectrum is that when processed into a freestanding film, water diffusion is kinetically limited. In particular, water is absorbed volumetrically (3D process) in the case of the powdered sample whereas the polymer film is subjected only to areal water uptake (2D process). Thus, the films absorb significantly less water from the atmosphere compared to the powder sample. This was evidenced by elemental analysis of the freestanding films of BBL-P, which revealed a total of ~2 water molecules per repeat unit. This is in contrast to the powder sample, which showed ~3 water molecules per repeat unit. The observed FTIR and Raman spectra data are in good agreement with previous reports of the parent BBL ladder polymer⁶⁵ and provide strong evidence for the molecular structure of BBL-P.

Electronic Structure and Optical Properties. We investigated the electronic structure of BBL-P by density functional theory (DFT) calculations, time-dependent DFT (TD-DFT) calculations, and cyclic voltammetry in conjunction with optical absorption spectroscopy. The DFT calculations were performed at the ω B97XD/6-31G(d,p) level of theory for a BBL-P oligomer comprising three repeat units to gain insight into the polymer conformation and frontier molecular orbital distribution (Figure 2). Note that a trimer was chosen to balance low computational costs and accuracy of simulation, and a trans-cis-trans conformation with respect to the imide was chosen to represent the polymer backbone, given that benzimidazobenzophenanthroline polymers are a statistical mixture of cis and trans repeat units. ^{19,70} The optimized

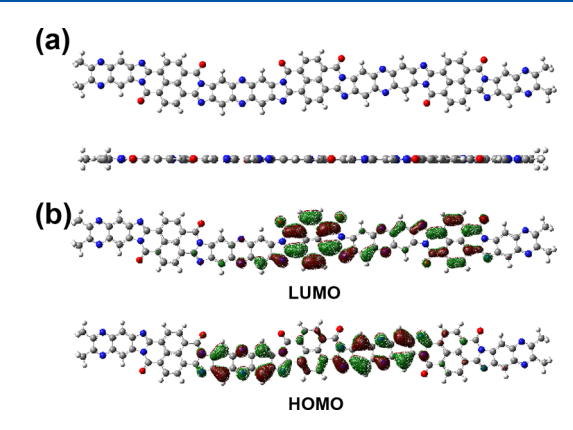


Figure 2. DFT calculations of (a) the optimized ground-state molecular geometry of BBL-P oligomer, and (b) pictorial representation of ground-state frontier molecular orbitals. Calculations were performed at the ω B97XD/6-31G(d,p) level of theory.

geometry is completely planar with a dihedral angle of 0.00° between the phenazine and naphthalene imide moieties (Figure 2a), which is similar to the observed molecular geometry of the parent BBL ladder polymer. The molecular orbital distributions of the HOMO and LUMO are distributed along the backbone, where the HOMO is concentrated on the phenazine moieties and the LUMO on the naphthalene imide moieties (Figure 2b). This spatial distribution suggests an enhanced intramolecular charge transfer (ICT) character in BBL-P compared to the parent polymer BBL that shows minimal spatial localizations of the HOMO molecular orbitals (Figure S3). The spatial of the HOMO molecular orbitals (Figure S3).

Excited-state transitions were calculated using time-dependent (TD) DFT at the same ω B97XD/6-31G(d,p) level of theory. The calculated absorption spectrum in Figure S4a closely resembles the experimental thin film absorption spectrum where the low-energy peak centered at 527 nm represents the $\pi-\pi^*$ transition. The pictorial representations of both the electron and hole orbital distributions associated with the $\pi-\pi^*$ transition are shown in Figure S4b.

The reorganization energy (λ) of BBL-P was calculated from the sum of the relaxation energies in the neutral and anionic states. The anionic geometry and orbital distribution of the oligomer are illustrated in Figure S4c. Reorganization energy can be described as the energy corresponding to structural changes when going from the neutral to the charged-state geometry; typically, the lower the reorganizational energy, the higher the charge transfer rate. The reorganization energy of 432 meV calculated for BBL-P is comparable to those calculated for conjugated rigid-rod polymers (327–427 meV) featuring isoindigo units using a similar level of theory and number of monomer units. Note that the calculated λ decreases with increasing number of monomers (n) and more accurate descriptions of the polymer chain would require n > 12.

We used cyclic voltammetry (CV) to measure the HOMO/LUMO energy levels of BBL-P, and the results are summarized in Table 2. The CVs for reduction and oxidation processes (Figure 3a,b) of BBL-P thin films coated on indium tin oxide (ITO) glass substrates were taken in 0.1 M tetrabutylammonium hexafluorophosphate (Bu_4NPF_6) in degassed acetonitrile with $Ag/AgNO_3$ as the reference electrode. BBL-P thin films showed two quasi-reversible reduction waves in the CV scans (Figure 3a), and these were accompanied by observed color

Table 2. Optical Properties and Electronic Structure of BBL-P and BBL

polymer	λ_{\max}^{a} (nm)	$\varepsilon_{\rm max}~({ m M}^{-1}~{ m cm}^{-1})$	λ_{\max}^{b} (nm)	$\alpha~(\times~10^5~{\rm cm}^{-1})$	$E_{\rm g}^{\;{ m opt.}c}\;({ m eV})$	$E_{\rm g}^{\rm opt.d}$ (eV)	HOMO (eV)	LUMO (eV)
BBL-P	512	3.7×10^4	474	1.4	1.64	1.62	-5.5	-4.0
BBL	545	4.3×10^{4}	574	1.9	1.70		-5.9^{e}	-4.0^{e}

^aAbsorption maximum in MSA solution. ^bSpin-coated thin films from MSA solution. ^cThin films on glass substrates. ^dFreestanding film. ^eValues taken from ref 10.

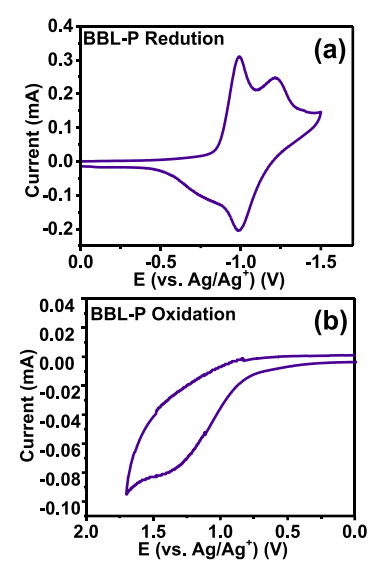


Figure 3. Cyclic voltammograms for the (a) reduction and (b) oxidation processes of BBL-P thin films measured in 0.1 M Bu_4NPF_6 electrolyte solution using $Ag/AgNO_3$ as the reference electrode. The scan rate was 100 mV/s.

changes in the film during the scans. In particular, the initial dark brown BBL-P film changed to dark purple at the first reduction process at -0.99 V, whereas the second reduction process at -1.22 V changed the film color to a bright orange. These electrochromic effects were found to be relatively stable, which is similar to the previous results for BBL thin films. The CV oxidation scans (Figure 3b) showed a non-reversible peak with no observable color changes. The onset oxidation potential and onset reduction potential of BBL-P are 0.85 V and -0.86 V, respectively, from which we estimated the HOMO level of -5.5 eV and LUMO level of -4.0 eV by using $E_{\text{LUMO}} = -(eE_{\text{red}}^{\text{onset}} + 4.8)$ and $E_{\text{HOMO}} = -(eE_{\text{ox}}^{\text{onset}} + 4.8)$. While the LUMO value is identical to that of the parent BBL, the HOMO value of BBL-P is increased by 0.4 eV (HOMO = -5.9 eV for BBL). ¹⁰ Although the expansion of the repeat unit of BBL by phenazine substitution has little impact on the LUMO energy levels, it has a large effect on the HOMO energy level; this means that when electronically coupled to the strong electron-withdrawing naphthalene imide moiety, the phenazine acts as an electron donor, thereby enhancing ICT interactions. This correlates well with the theoretical calculations showing localization of the HOMO wavefunctions on the phenazine core (Figure 2b).

The optical absorption spectrum of freestanding BBL-P film is shown in Figure 1e. It has a broad absorption band with a peak at 472 nm accompanied by weak vibronic features at 380 and 635 nm. We estimate the optical bandgap ($E_{\rm g}^{\rm opt}$) of the freestanding film to be 1.62 eV (Table 2). The optical absorption spectra of BBL-P in dilute MSA solution and as a thin film on a glass substrate are shown in Figure 4a,b, and the optical properties (molar absorptivity ($\varepsilon_{\rm max}$), absorption

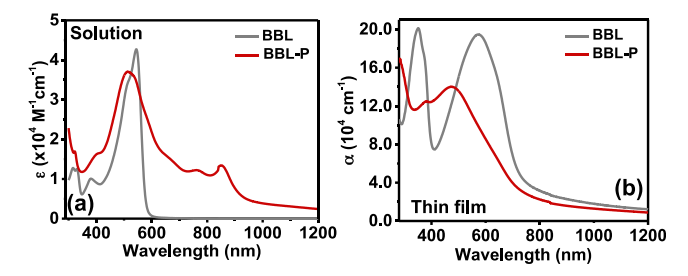


Figure 4. Absorption spectrum of BBL-P (red) and BBL (gray) in (a) dilute methanesulfonic acid solution and (b) thin film on the glass substrate.

coefficient (α), and optical bandgap ($E_{\rm g}^{\rm opt.}$)) are summarized in Table 2. In solution (Figure 4a), BBL-P has a broad absorption band with a peak at 512 nm ($\varepsilon_{\rm max}=3.7\times10^4~{\rm M}^{-1}~{\rm cm}^{-1}$) and a lower intensity peak at 840 nm ($\varepsilon_{\rm max}=1.3\times10^4~{\rm M}^{-1}~{\rm cm}^{-1}$). To help in understanding the unusual line shape of the absorption spectrum of BBL-P in MSA solution, we also show the absorption spectrum of BBL in MSA solution in Figure 4a. A relatively narrow absorption band with a peak at 545 nm ($\varepsilon_{\rm max}=4.3\times10^4~{\rm M}^{-1}~{\rm cm}^{-1}$) is seen in the parent BBL. We propose that the 840 nm absorption band in the MSA solution spectrum of BBL-P is due to intramolecular charge transfer (ICT), 76 enhanced by protonation of the imine nitrogens of the phenazine moieties. This interpretation is in agreement with similar observations in acid solutions of imine nitrogen-containing π -conjugated polymers 77 as well as with the previously discussed DFT calculations.

The thin film absorption spectrum of BBL-P (Figure 4b) is a broad band in the 300-700 nm range with a peak centered at 474 nm and absorption coefficient of 1.4×10^5 cm⁻¹. The optical bandgap $(E_{\rm g}^{\rm \ opt.})$ measured from the onset of the BBL-P thin film absorption spectrum is 1.64 eV, which is identical to the bandgap measured from the freestanding BBL-P film (Figure 1e). Compared to the solution absorption spectrum, the thin film absorption spectrum is markedly different in line shape. Notably, the 840 nm absorption peak observed in the solution spectrum is absent in the solid state, confirming its protonation-induced ICT origin. The main absorption peak of BBL-P, which is due to the π - π * transition, centered at 512 nm in the solution spectrum is significantly blue shifted to 474 nm in the solid state (Table 2). It is tempting to interpret the blue shift of the thin film absorption spectrum of BBL-P relative to its solution as a consequence of H-aggregation in the solid state. 78,79 However, an alternative interpretation is that the difference originates in differences in backbone conformation in solution and the solid state; 80 in this case, the protonated polymer chains in solution would presumably be more planar than the neutral polymer chains in the thin film.

The MSA solution and thin film optical absorption spectra of BBL, the parent ladder polymer, are shown in Figure 4a,b, respectively, for comparison with those of BBL-P. There are clearly dramatic differences in both the solution and solid-state absorption spectra. It is to be noted that BBL does not absorb

above 600 nm in MSA solution, and this further confirms that the 840 nm absorption band in BBL-P solution originates from protonation of the phenazine moieties. Furthermore, in solution, the BBL-P absorption maximum ($\lambda_{\rm max}=512$ nm) is 33 nm blue-shifted relative to BBL but the two ladder polymers have comparable $\varepsilon_{\rm max}$ (Table 2). Although BBL-P has a slightly narrower optical bandgap ($E_{\rm g}^{\rm opt.}=1.64$ eV) than BBL ($E_{\rm g}^{\rm opt.}=1.70$ eV), there is a large difference in the solid-state absorption maxima of 574 nm in BBL versus 474 nm in BBL-P (Table 2). The slow rise of absorption from the edge to the absorption maximum in BBL-P is indicative of a more disordered organic semiconductor compared to BBL with a sharp rise in absorption (Figure 4b).

Thin Film Morphology. Atomic force microscopy (AFM) imaging and two-dimensional grazing-incidence wide-angle X-ray scattering (2D-GIWAXS) are used to characterize the surface morphology and bulk morphology of BBL-P films, respectively. AFM height and phase images of BBL-P are shown in Figure S5a,b, whereas the 2D GIWAXS diffraction patterns and 1D line cuts for BBL-P films are presented in Figure 5. The peak positions, lamellar spacing, $\pi - \pi$ stacking distance, and crystalline coherence length (L_c) are summarized in Table S1.

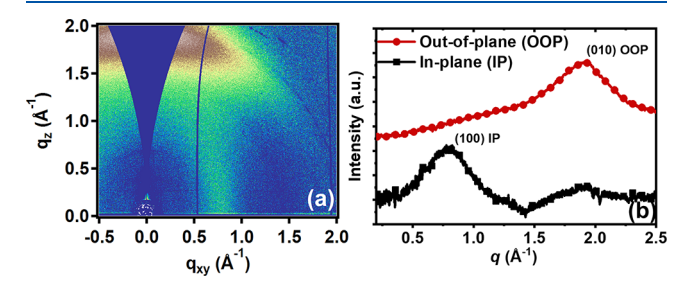


Figure 5. (a) 2D-GIWAXS diffraction pattern of BBL-P thin film and (b) 1D line cuts of GIWAXS patterns in the out-of-plane (OOP) direction and the in-plane (IP) direction.

Films of BBL-P showed a featureless and smooth surface (Figure S5a,b) with a root-mean-square roughness of 1.6 nm in AFM imaging, suggesting a relatively low degree of polymer crystallinity. BBL-P films exhibited a pronounced (100) diffraction peak in the in-plane (IP) direction at q_{xy} of 0.78 Å-1, which corresponds to a lamellar spacing of 8.03 Å (Table S1). We note that the lamellar packing distance of BBL-P is slightly smaller than that of BBL (8.4 Å), 16 which can be rationalized by the strong intermolecular interactions between the imine nitrogens on the phenazine units. In the out-of-plane (OOP) direction, the BBL-P thin film showed an intense (010) diffraction peak at q_z of 1.90 $\mbox{\normalfont\AA}^{-1}$ resulting in a $\pi{-}\pi$ stacking distance of 3.31 Å, which is comparable to a $\pi - \pi$ stacking distance of 3.34 Å for BBL thin films. 16 The presence of the (100) IP diffraction peak and the (010) OOP diffraction peak collectively suggests that most BBL-P crystallites preferentially adopt face-on orientations with respect to the substrate. Furthermore, the crystalline coherence lengths (L_c) of BBL-P in the (100) IP and (010) OOP directions were found to be 1.07 and 1.04 nm, respectively, which is significantly lower than those of BBL (~12 nm and ~25 nm) even at the lowest polymer molecular weight. 16 Thus, substitution of the phenazine moiety for the benzene moiety in the polymer backbone not only renders the BBL-P polymer more amorphous but also changes the molecular orientations

from preferentially edge-on in BBL¹⁶ to preferentially face-on in BBL-P, both of which have implications for field-effect electron transport of BBL-P thin films.

Field-Effect Charge Transport Properties. We investigated the electron transport properties of the BBL-P ladder polymer by fabricating and characterizing n-channel organic field-effect transistors (OFETs). The transistors were fabricated in a bottom-gate/top-contact device architecture with channel dimensions of 100 μ m/1000 μ m (length/width). A thin polystyrene buffer layer was used to passivate silanol charge trapping sites on silicon dioxide surfaces. 19,81 The presence of a low dielectric constant buffer layer has been previously demonstrated to reduce the number of charge trapping groups and energetic expense from the charge carrierdipole interactions in BBL OFETs. 19,81 The capacitance per unit area of the gate dielectric was calculated from the dielectric constants and thickness of the layers to be 10.6 nF/ cm². Representative output and transfer curves are presented in Figure 6, and the transistors parameters are summarized in Table S2.

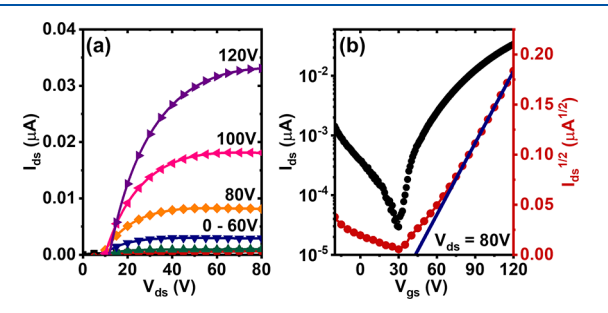


Figure 6. (a) Representative output curves of the BBL-P n-channel organic field-effect transistor with a channel length/channel width of $100~\mu m/1000~\mu m$. (b) Representative transfer curve of the BBL-P transistor.

The n-channel BBL-P OFETs showed reasonable current modulation with good saturation (Figure 6a) and minimal hysteresis (Figure S6). The average saturation region fieldeffect electron mobility (μ_{FET}) of BBL-P in a nitrogen atmosphere was found to be $(9.60 \pm 1.58) \times 10^{-5} \text{ cm}^2/\text{V} \text{ s.}$ The maximum $\mu_{\rm FET}$ value of BBL-P on the polystyrene buffer layer was $1.21 \times 10^{-4}~{\rm cm^2/V}$ s (Table S2), which is about two orders of magnitude lower than that of BBL measured using the same device configuration.¹⁹ The observed lower electron mobility of BBL-P is partly due to the lower polymer molecular weight as exemplified by the low intrinsic viscosity ($[\eta] \sim 0.7$ dL/g in MSA at 30.0 °C) compared to that of the previously reported value for BBL ([η] ~ 7.0 dL/g in MSA at 30.0 °C). 16,19 The modest field-effect electron mobility of BBL-P can also be attributed to poor polymer crystallinity as well as the predominantly face-on molecular orientations observed in the thin film microstructure. The average on/off current ratio was $(7.7 \pm 3.4) \times 10^2$, whereas the average threshold voltage was 45.1 ± 1.72 V. We note that improved electron mobility, higher on/off current ratio, and lower threshold voltage can be achieved by further increasing BBL-P molecular weights to not only enhance the polymer crystallinity but also increase the volume fraction of edge-on oriented crystallites.10

Mechanical Properties of BBL-P Thin Films. We also investigated the mechanical properties of BBL-P ladder polymers by using the nanoindentation technique. The nanoindentation test enabled local probing of the dynamic

mechanical properties of BBL-P films, which could be more sensitive than dynamic mechanical analysis of bulk samples. The nanoindentation measurements were carried out in a constant displacement mode whereby three indents were made across the film surface at each indent depth. The total BBL-P film thickness was determined by a profilometer to be around 650 nm, which was sufficiently thick to assume that the measured mechanical properties are intrinsic to BBL-P film without any substrate interference. The load profiles (Figure S7f) consisted of three processes including 5 s of loading, 30 s of holding to allow creep effects to settle, and 5 s of unloading. The response load—displacement curve is presented in Figure S7g. The AFM topography images of the BBL-P film surface collected after each measurement (Figures S7a—e) showed distinct indent marks.

As presented in Figure 7a, the elastic modulus of BBL-P thin films varied marginally between 13 and 20% indent depth into

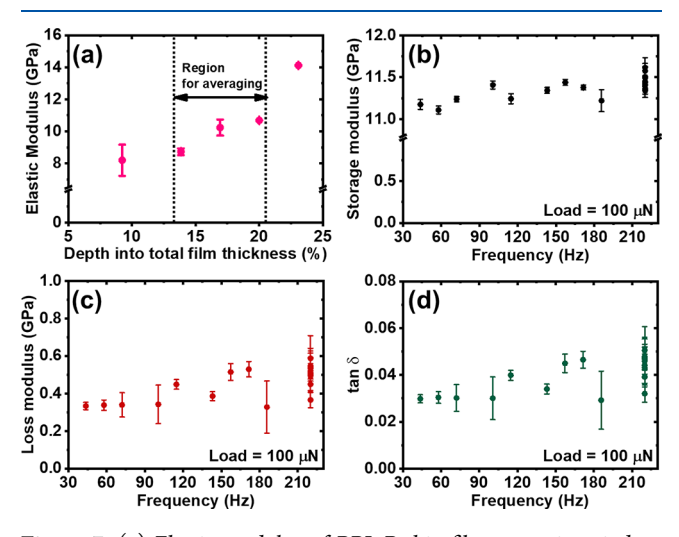


Figure 7. (a) Elastic modulus of BBL-P thin films at various indent depths measured by nanoindentation tests. (b-d) Dynamic mechanical properties of BBL-P thin films as a function of frequency measured at room temperature by nano(dynamic mechanical analysis): (b) storage modulus, (c) loss modulus, and (d) loss tangent (tan δ).

the total film thickness while values outside this range are likely to be either underestimated (<10%) due to the "skin effect" or overestimated due to substrate effects (>20%). Thus, the elastic modulus of BBL-P thin film was found to be 10 GPa, which was averaged from the moduli in the range of 13–20% into the film thickness. The elastic modulus of BBL-P was a few times higher than that of other non-ladder conjugated polymers (0.7–2.7 GPa), $^{84-88}$ indicating the superior mechanical properties of rigid-rod ladder polymers.

The dynamic mechanical properties of BBL-P thin films were also investigated by applying a sinusoidal load profile using the nanoindentation probe with an amplitude of $100~\mu N$ at varying frequencies from 45 to 200 Hz, and the results are shown in Figure 7b–d. The storage modulus (E') of BBL-P polymers was found to be around 11 GPa and independent of the applied frequency. Similar behavior was also observed for the loss modulus (E'') (Figure 7c) as a function of the applied frequency. The order of magnitude higher E' values of BBL-P compared to semiflexible conjugated polymers measured using the same technique accompanied by the relatively constant E' and E'' are indicative of the superior mechanical robustness of

the class of rigid-rod ladder polymers. This observation is further confirmed by the small loss tangent (tan $\delta < 0.05$) (Figure 7d), which indicates that the BBL-P polymer behaves as a nearly elastic material in contrast to other non-ladder conjugated polymers. Furthermore, the near-zero tan δ values allow the approximation of Young's modulus of BBL-P to be ~11 GPa.

To place the observed elastic modulus of BBL-P in context, we also performed nanoindentation tests on the parent BBL ladder polymer as a check. The average elastic modulus of BBL film ($E_{\rm BBL}$) was found to be 7.9 \pm 0.4 GPa, which is within a reasonable range of reported values. ^{89,90} An elastic modulus of about 4 GPa was reported for a BBL filter cake (25 mm) via dynamic mechanical analysis ⁸⁹ while that of heat-treated highly oriented BBL fibers was found to be 120 GPa. ⁹⁰

CONCLUSIONS

We have synthesized and for the first time investigated the electronic structure, thin film morphology, field-effect electron transport, and optical and mechanical properties of phenazines ubstituted ladder poly(benzimidazobenzophenanthrolinedione), BBL-P. Although the measured intrinsic viscosity ([η]) of 1.1 dL/g in concentrated H₂SO₄ implies a moderate molecular weight, the BBL-P sample could form strong and flexible freestanding films. In MSA solution, the BBL-P absorption spectrum showed an additional long-wavelength peak at 840 nm, which is absent in the spectrum of BBL and is attributed to an intramolecular charge transfer (ICT) band enabled by protonation of the phenazine moiety in BBL-P. Our characterization of the mechanical properties of BBL-P films by nanoindentation technique gave a high Young modulus of 11 GPa.

BBL-P thin films have an optical bandgap of 1.6 eV, which is slightly reduced relative to that of BBL (1.7 eV). GIWAXS characterization of the thin film microstructure of BBL-P showed that the degree of crystallinity is reduced and the predominant molecular orientation (face-on) is different compared to reported BBL thin films (edge-on). We found the LUMO energy level of BBL-P thin films (-4.0 eV) to be identical to that of BBL; however, the measured HOMO energy level of -5.5 eV is significantly elevated compared to BBL (-5.9 eV). BBL-P based n-channel OFETs had an average electron mobility of $1.0 \times 10^{-4} \text{ cm}^2/\text{V}$ s, which is about two orders of magnitude less than in BBL 19 likely due to the reduced molecular weight, reduced crystallinity, and unfavorable face-on molecular orientations of BBL-P. The present results on BBL-P provide important new insights into how the backbone chain structure of π -conjugated polymers influences the electronic structure, thin film morphology, and optical and charge transport properties. Further investigations of the performance of BBL-P polymer as an n-channel material of OECTs will be intriguing as lower crystallinity and the hygroscopic nature of BBL-P may be beneficial to OECT operation. 91,92

ASSOCIATED CONTENT

5 Supporting Information

The Supporting Information is available free of charge at https://pubs.acs.org/doi/10.1021/acs.macromol.2c01999.

Fabrication of thin films and freestanding films of BBL-P, TGA, and DSC scans, DFT calculated excited state and anionic geometries and wavefunctions, DFT-

calculated BBL HOMO/LUMO orbital distributions, simulated UV-Vis absorption spectrum and electron and hole orbital pictorial representations, AFM images, transfer curves of transistors, load profile and load—displacement curve, field-effect charge transport properties, and GIWAXS parameters (PDF)

AUTHOR INFORMATION

Corresponding Author

Samson A. Jenekhe — Department of Chemistry and Department of Chemical Engineering, University of Washington, Seattle, Washington 98195-1750, United States; © orcid.org/0000-0002-0898-9541; Email: jenekhe@u.washington.edu

Authors

Sarah M. West – Department of Chemistry, University of Washington, Seattle, Washington 98195-1750, United States

Duyen K. Tran – Department of Chemical Engineering, University of Washington, Seattle, Washington 98195-1750, United States; Oorcid.org/0000-0002-3065-6153

Jiajie Guo — Molecular Engineering and Science Institute, University of Washington, Seattle, Washington 98195, United States; Oorcid.org/0000-0001-9131-4352

Shinya E. Chen — Molecular Engineering and Science Institute, University of Washington, Seattle, Washington 98195, United States; orcid.org/0000-0001-8995-7500

David S. Ginger — Department of Chemistry, University of Washington, Seattle, Washington 98195-1750, United States; Occid.org/0000-0002-9759-5447

Complete contact information is available at: https://pubs.acs.org/10.1021/acs.macromol.2c01999

Notes

The authors declare no competing financial interest.

ACKNOWLEDGMENTS

This work was supported by the National Science Foundation (DMR-2003518). J.G., S.E.C., and D.S.G. acknowledge support from NSF DMR-2003456. Part of this work was conducted at the Molecular Analysis Facility, a National Nanotechnology Coordinated Infrastructure (NNCI) site at the university of Washington with partial support from the National Science Foundation via awards NNCI-2025489 and NNCI-1542101. Part of this work was conducted using equipment in the Biomedical Diagnostic Foundry for Translational Research sponsored by the M.J. Murdock Charitable Trust. The DFT calculations were done through the use of advanced computational, storage, and networking infrastructure provided by the Hyak supercomputer system at the University of Washington. This research used beamline 7.3.3⁶² of the Advanced Light Source (ALS), which is a DOE Office of Science User Facility under contract no. DEAC02-05CH11231. The authors thank C. Zhu and E. Schaible at the ALS for assistance with GIWAXS data acquisition and analysis.

REFERENCES

- (1) Deusen, R. L. V. Benzimidazo-Benzophenanthroline Polymers. *J. Polym. Sci. B Polym. Lett.* **1966**, *4*, 211–214.
- (2) Shirakawa, H.; Louis, E. J.; MacDiarmid, A. G.; Chiang, C. K.; Heeger, A. J. Synthesis of Electrically Conducting Organic Polymers:

ı

- Halogen Derivatives of Polyacetylene, (CH)x. J. Chem. Soc., Chem. Commun. 1977, 578-580.
- (3) Kim, O.-K. Ladder Polymers as New Polymeric Conductors. *Mol. Cryst.* **1984**, *105*, 161–173.
- (4) Wilbourn, K.; Murray, R. W. The Electrochemical Doping Reactions of the Conducting Ladder Polymer Benzimidazobenzophenanthroline (BBL). *Macromolecules* **1988**, *21*, 89–96.
- (5) Jenekhe, S. A.; Tibbetts, S. J. Ion Implantation Doping and Electrical Properties of High-Temperature Ladder Polymers. *J. Polym. Sci., Part B: Polym. Phys.* **1988**, *26*, 201–209.
- (6) Osaheni, J. A.; Jenekhe, S. A.; Burns, A.; Du, G.; Joo, J. S.; Wang, Z. H.; Epstein, A. J.; Wang, C. S. Spectroscopic and Morphological Studies of Highly Conducting Ion-Implanted Rigid-Rod and Ladder Polymers. *Macromolecules* **1992**, 25, 5828–5835.
- (7) Wang, Z. H.; Du, G.; Joo, J.; Burns, A.; Jasty, S.; Zhou, P.; Epstein, A. J.; Osaheni, J. A.; Jenekhe, S. A.; Wang, C. S. Weak-Localization, Electron-Electron Interaction, and Metal-Insulator-Transition in Ion-Implanted Polymers. *Synth. Met.* **1993**, *57*, 4829–4835
- (8) Babel, A.; Jenekhe, S. A. Electron Transport in Thin-Film Transistors From an n-Type Conjugated Polymer. *Adv. Mater.* **2002**, *14*, 371–374.
- (9) Babel, A.; Jenekhe, S. A. N-Channel Field-Effect Transistors from Blends of Conjugated Polymers. *J. Phys. Chem. B* **2002**, *106*, 6129–6132.
- (10) Alam, M. M.; Jenekhe, S. A. Conducting Ladder Polymers: Insulator-to-Metal Transition and Evolution of Electronic Structure upon Protonation by Poly(Styrenesulfonic Acid). *J. Phys. Chem. B* **2002**, *106*, 11172–11177.
- (11) Babel, A.; Jenekhe, S. A. High Electron Mobility in Ladder Polymer Field-Effect Transistors. *J. Am. Chem. Soc.* **2003**, *125*, 13656–13657.
- (12) Alam, M. M.; Jenekhe, S. A. Efficient Solar Cells from Layered Nanostructures of Donor and Acceptor Conjugated Polymers. *Chem. Mater.* **2004**, *16*, 4647–4656.
- (13) Jenekhe, S. A.; Yi, S. Efficient Photovoltaic Cells from Semiconducting Polymer Heterojunctions. *Appl. Phys. Lett.* **2000**, 77, 2635–2637.
- (14) Sun, H.; Vagin, M.; Wang, S.; Crispin, X.; Forchheimer, R.; Berggren, M.; Fabiano, S. Complementary Logic Circuits Based on High-Performance n-Type Organic Electrochemical Transistors. *Adv. Mater.* **2018**, *30*, 1704916.
- (15) Surgailis, J.; Savva, A.; Druet, V.; Paulsen, B. D.; Wu, R.; Hamidi-Sakr, A.; Ohayon, D.; Nikiforidis, G.; Chen, X.; McCulloch, I.; Rivnay, J.; Inal, S. Mixed Conduction in an N-Type Organic Semiconductor in the Absence of Hydrophilic Side-Chains. *Adv. Funct. Mater.* **2021**, *31*, 2010165.
- (16) Wu, H.-Y.; Yang, C.-Y.; Li, Q.; Kolhe, N. B.; Strakosas, X.; Stoeckel, M.-A.; Wu, Z.; Jin, W.; Savvakis, M.; Kroon, R.; Tu, D.; Woo, H. Y.; Berggren, M.; Jenekhe, S. A.; Fabiano, S. Influence of Molecular Weight on the Organic Electrochemical Transistor Performance of Ladder-Type Conjugated Polymers. *Adv. Mater.* 2022, 34, 2106235.
- (17) Babel, A.; Wind, J. D.; Jenekhe, S. A. Ambipolar Charge Transport in Air-Stable Polymer Blend Thin-Film Transistors. *Adv. Funct. Mater.* **2004**, *14*, 891–898.
- (18) Kim, F. S.; Ahmed, E.; Subramaniyan, S.; Jenekhe, S. A. Air-Stable Ambipolar Field-Effect Transistors and Complementary Logic Circuits from Solution-Processed n/p Polymer Heterojunctions. *ACS Appl. Mater. Interfaces* **2010**, *2*, 2974–2977.
- (19) Kim, F. S.; Park, C. H.; Na, Y.; Jenekhe, S. A. Effects of Ladder Structure on the Electronic Properties and Field-Effect Transistor Performance of Poly(Benzobisimidazobenzophenanthroline). *Org. Electron.* **2019**, *69*, 301–307.
- (20) Wang, S.; Sun, H.; Ail, U.; Vagin, M.; Persson, P. O. Å.; Andreasen, J. W.; Thiel, W.; Berggren, M.; Crispin, X.; Fazzi, D.; Fabiano, S. Thermoelectric Properties of Solution-Processed n-Doped Ladder-Type Conducting Polymers. *Adv. Mater.* **2016**, 28, 10764–10771.

- (21) Tam, T. L. D.; Lin, M.; Handoko, A. D.; Lin, T. T.; Xu, J. High-Performance & Thermally Stable n-Type Polymer Thermoelectrics Based on a Benzyl Viologen Radical Cation-Doped Ladder-Type Conjugated Polymer. *J. Mater. Chem. A* **2021**, *9*, 11787–11793.
- (22) Yang, C. Y.; Stoeckel, M. A.; Ruoko, T. P.; Wu, H. Y.; Liu, X.; Kolhe, N. B.; Wu, Z.; Puttisong, Y.; Musumeci, C.; Massetti, M.; Sun, H.; Xu, K.; Tu, D.; Chen, W. M.; Woo, H. Y.; Fahlman, M.; Jenekhe, S. A.; Berggren, M.; Fabiano, S. A High-Conductivity n-Type Polymeric Ink for Printed Electronics. *Nat. Commun.* **2021**, *12*, 2345.
- (23) Volkov, A. V.; Sun, H.; Kroon, R.; Ruoko, T.-P.; Che, C.; Edberg, J.; Muller, C.; Fabiano, S.; Crispin, X. Asymmetric Aqueous Supercapacitor Based on P- and n-Type Conducting Polymers. *ACS Appl. Energy Mater.* **2019**, *2*, 5350–5355.
- (24) Xu, K.; Sun, H.; Ruoko, T.-P.; Wang, G.; Kroon, R.; Kolhe, N. B.; Puttisong, Y.; Liu, X.; Fazzi, D.; Shibata, K.; Yang, C.-Y.; Sun, N.; Persson, G.; Yankovich, A. B.; Olsson, E.; Yoshida, H.; Chen, W. M.; Fahlman, M.; Kemerink, M.; Jenekhe, S. A.; Müller, C.; Berggren, M.; Fabiano, S. Ground-State Electron Transfer in All-Polymer Donor—Acceptor Heterojunctions. *Nat. Mater.* **2020**, *19*, 738–744.
- (25) Cheng, P.; Zhao, X.; Zhan, X. Perylene Diimide-Based Oligomers and Polymers for Organic Optoelectronics. *Acc. Mater. Res.* **2022**, *3*, 309–318.
- (26) Li, C.; Wonneberger, H. Perylene Imides for Organic Photovoltaics: Yesterday, Today, and Tomorrow. *Adv. Mater.* **2012**, 24, 613–636.
- (27) Zhou, N.; Facchetti, A. Naphthalenediimide (NDI) Polymers for All-Polymer Photovoltaics. *Mater. Today* **2018**, *21*, 377–390.
- (28) Sommer, M. Conjugated Polymers Based on Naphthalene Diimide for Organic Electronics. *J. Mater. Chem. C* **2014**, *2*, 3088–3098
- (29) Zhan, X.; Facchetti, A.; Barlow, S.; Marks, T. J.; Ratner, M. A.; Wasielewski, M. R.; Marder, S. R. Rylene and Related Diimides for Organic Electronics. *Adv. Mater.* **2011**, 23, 268–284.
- (30) Kumar, S.; Shukla, J.; Kumar, Y.; Mukhopadhyay, P. Electron-Poor Arylenediimides. *Org. Chem. Front.* **2018**, *5*, 2254–2276.
- (31) Guo, X.; Tu, D.; Liu, X. Recent Advances in Rylene Diimide Polymer Acceptors for All-Polymer Solar Cells. *J. Energy Chem.* **2015**, 24, 675–685.
- (32) Fuktomi, Y.; Nakano, M.; Hu, J. Y.; Osaka, I.; Takimiya, K. Naphthodithiophenediimide (NDTI): Synthesis, Structure, and Applications. *J. Am. Chem. Soc.* **2013**, *135*, 11445–11448.
- (33) Imai, K.; Kurihara, M.; Mathias, L.; Wittmann, J.; Alston, W. B.; Stille, J. K. Synthesis and Properties of Thermally Stable Ladder Polymers Containing the 1,4-Pyrazine Ring Obtained from Polyheterocyclizations of Tetramines and Tetraketones in Poly-(Phosphoric Acid) and m-Cresol. *Macromolecules* 1973, 6, 158–162.
- (34) Sicree, A. J.; Arnold, F. E.; Deusen, R. L. V. New Imidazoisoquinoline Ladder Polymers. *J. Polym. Sci. Polym. Chem.* 1974, 12, 265–272.
- (35) Gerber, A. H. Thermally Stable Polymers Derived from 2,3,5,6-Tetraaminopyridine. *J. Polym. Sci. Polym. Chem.* **1973**, *11*, 1703–1719
- (36) Hirvonen, S.; Tenhu, H. Modification of Naphthalenic Unit in BBL Main Chain. *Synth. Met.* **2015**, 207, 87–95.
- (37) Arnold, F. E. Ladder Polymers from Tetraaminodiquinoxalpyrene. J. Polym. Sci., Part A: Polym. Chem. 1970, 8, 2079–2089.
- (38) Tonzola, C. J.; Alam, M. M.; Kaminsky, W.; Jenekhe, S. A. New N-Type Organic Semiconductors: Synthesis, Single Crystal Structures, Cyclic Voltammetry, Photophysics, Electron Transport, and Electroluminescence of a Series of Diphenylanthrazolines. *J. Am. Chem. Soc.* 2003, 125, 13548–13558.
- (39) Mortensen, J.; Heinze, J. The Electrochemical Reduction of Benzene—First Direct Determination of the Reduction Potential. *Angew. Chem., Int. Ed.* **1984**, 23, 84–85.
- (40) Kim, D. H.; Han, Y. W.; Moon, D. K. A Comparative Investigation of Dibenzo[a,c]Phenazine and Quinoxaline Donor–Acceptor Conjugated Polymers: Correlation of Planar Structure and Intramolecular Charge Transfer Properties. *Polymer* **2019**, *185*, No. 121906.

- (41) Zhang, Y.; Zou, Y.; Yip, H. L.; Chen, K. S.; Zeigler, D. F.; Sun, Y.; Jen, A. K. Y. Indacenodithiophene and Quinoxaline-Based Conjugated Polymers for Highly Efficient Polymer Solar Cells. *Chem. Mater.* **2011**, 23, 2289–2291.
- (42) He, R.; Yu, L.; Cai, P.; Peng, F.; Xu, J.; Ying, L.; Chen, J.; Yang, W.; Cao, Y. Narrow-Band-Gap Conjugated Polymers Based on 2,7-Dioctyl-Substituted Dibenzo[a,c]Phenazine Derivatives for Polymer Solar Cells. *Macromolecules* **2014**, *47*, 2921–2928.
- (43) Kim, J. H.; Song, C. E.; Kim, H. U.; Kang, I.-N.; Shin, W. S.; Park, M. J.; Hwang, D. H. New Quinoxaline Derivatives as Accepting Units in Donor—Acceptor Type Low-Band Gap Polymers for Organic Photovoltaic Cells. *J. Polym. Sci., Part A: Polym. Chem.* **2013**, *51*, 4136–4149.
- (44) Fan, Q.; Liu, Y.; Xiao, M.; Tan, H.; Wang, Y.; Su, W.; Yu, D.; Yang, R.; Zhu, W. Donor—Acceptor Copolymers Based on Benzo[1,2-b:4,5-B']Dithiophene and Pyrene-Fused Phenazine for High-Performance Polymer Solar Cells. *Org. Electron.* **2014**, *15*, 3375—3383.
- (45) Li, Y.; Fu, Y.; Tong, H.; Xie, Z.; Wang, L. Effect of Side-Chain Positions on Morphology and Photovoltaic Properties of Phenazine-Based Donor-Acceptor Copolymers. J. Polym. Sci., Part A: Polym. Chem. 2013, 51, 2910–2918.
- (46) Li, G.; Lu, Z.; Li, C.; Bo, Z. The Side Chain Effect on Difluoro-Substituted Dibenzo[a,c]Phenazine Based Conjugated Polymers as Donor Materials for High Efficiency Polymer Solar Cell. *Polym. Chem.* **2015**, *6*, 1613–1618.
- (47) Wang, K.; Jiang, P.; Zhang, Z. G.; Fu, Q.; Li, Y. Synthesis and Photovoltaic Properties of D-A Copolymers Based on 11,12-Difluorodibenzo[a,c]Phenazine Acceptor Unit. *Macromol. Chem. Phys.* **2013**, 214, 1772–1779.
- (48) Zhu, Y.; Gibbons, K. M.; Kulkarni, A. P.; Jenekhe, S. A. Polyfluorenes Containing Dibenzo[a,c]Phenazine Segments: Synthesis and Efficient Blue Electroluminescence from Intramolecular Charge Transfer States. *Macromolecules* **2007**, *40*, 804–813.
- (49) Li, Y.; Meng, B.; Tong, H.; Xie, Z.; Wang, L. A Chlorinated Phenazine-Based Donor—Acceptor Copolymer with Enhanced Photovoltaic Performance. *Polym. Chem.* **2014**, *5*, 1848—1851.
- (50) Zhang, J.; Cai, W.; Huang, F.; Wang, E.; Zhong, C.; Liu, S.; Wang, M.; Duan, C.; Yang, T.; Cao, Y. Synthesis of Quinoxaline-Based Donor–Acceptor Narrow-Band-Gap Polymers and Their Cyclized Derivatives for Bulk-Heterojunction Polymer Solar Cell Applications. *Macromolecules* **2011**, *44*, 894–901.
- (51) Li, S.; He, Z.; Yu, J.; Chen, S.; Zhong, A.; Tang, R.; Wu, H.; Qin, J.; Li, Z. How the Linkage Positions Affect the Performance of Bulk-Heterojunction Polymer Solar Cells. *J. Mater. Chem.* **2012**, 22, 12523–12531.
- (52) Zhang, X.; Won Shim, J.; Prakash Tiwari, S.; Zhang, Q.; Norton, J. E.; Wu, P.-T.; Barlow, S.; Jenekhe, S. A.; Kippelen, B.; Brédas, J. L.; Marder, S. M. Dithienopyrrole Quinoxaline / Pyridopyrazine Donor—Acceptor Polymers: Synthesis and Electrochemical, Optical, Charge-Transport, and Photovoltaic Properties. J. Mater. Chem. 2011, 21, 4971—4982.
- (53) Izumi, A.; Nomura, R.; Masuda, T. Synthesis of A New Class of N-Dopable and Photoluminescent Conjugated Polymers Having Phenazine Units in the Main Chain. *Macromolecules* **2000**, *33*, 8918–8920.
- (54) Bischak, C. G.; Flagg, L. Q.; Yan, K.; Li, C.-Z.; Ginger, D. S. Fullerene Active Layers for N-Type Organic Electrochemical Transistors. ACS Appl. Mater. Interfaces 2019, 11, 28138–28144.
- (55) Savva, A.; Ohayon, D.; Surgailis, J.; Paterson, A. F.; Hidalgo, T. C.; Chen, X.; Maria, I. P.; Paulsen, B. D.; Petty, A. J., II; Rivnay, J.; McCulloch, I.; Inal, S. Solvent Engineering for High-Performance n-Type Organic Electrochemical Transistors. *Adv. Electron. Mater.* **2019**, *5*, 1900249.
- (56) Feng, K.; Shan, W.; Wang, J.; Lee, J.-W.; Yang, W.; Wu, W.; Wang, Y.; Kim, B. J.; Guo, X.; Guo, H. Cyano-Functionalized n-Type Polymer with High Electron Mobility for High-Performance Organic Electrochemical Transistors. *Adv. Mater.* **2022**, *34*, 2201340.
- (57) Moser, M.; Hidalgo, T. C.; Surgailis, J.; Gladisch, J.; Ghosh, S.; Sheelamanthula, R.; Thiburce, Q.; Giovannitti, A.; Salleo, A.;

- Gasparini, N.; Wadsworth, A.; Zozoulenko, I.; Berggren, M.; Stavrinidou, E.; Inal, S.; McCulloch, I. Side Chain Redistribution as a Strategy to Boost Organic Electrochemical Transistor Performance and Stability. *Adv. Mater.* **2020**, *32*, 2002748.
- (58) Chen, S. E.; Flagg, L. Q.; Onorato, J. W.; Richter, L. J.; Guo, J.; Luscombe, C. K.; Ginger, D. S. Impact of Varying Side Chain Structure on Organic Electrochemical Transistor Performance: A Series of Oligoethylene Glycol-Substituted Polythiophenes. *J. Mater. Chem. A* 2022, *10*, 10738–10749.
- (59) Moser, M.; Savva, A.; Thorley, K.; Paulsen, B. D.; Hidalgo, T. C.; Ohayon, D.; Chen, H.; Giovannitti, A.; Marks, A.; Gasparini, N.; Wadsworth, A.; Rivnay, J.; Inal, S.; McCulloch, I. Polaron Delocalization in Donor–Acceptor Polymers and Its Impact on Organic Electrochemical Transistor Performance. *Angew. Chem., Int. Ed.* **2021**, *60*, 7777–7785.
- (60) Deusen, R. L. V.; Goins, O. K.; Sicree, A. J. Thermally Stable Polymers from 1,4,5,8-Naphthalenetetracarboxylic Acid and Aromatic Tetraamines. *J. Polym. Sci., Part A-1: Polym. Chem.* **1968**, *6*, 1777–1793.
- (61) Oosterhout, S. D.; Savikhin, V.; Zhang, J.; Zhang, Y.; Burgers, M. A.; Marder, S. R.; Bazan, G. C.; Toney, M. F. Mixing Behavior in Small Molecule:Fullerene Organic Photovoltaics. *Chem. Mater.* **2017**, 29, 3062–3069.
- (62) Hexemer, A.; Bras, W.; Glossinger, J.; Schaible, E.; Gann, E.; Kirian, R.; MacDowell, A.; Church, M.; Rude, B.; Padmore, H. A SAXS/WAXS/GISAXS Beamline with Multilayer Monochromator. *J. Phys.: Conf. Ser.* **2010**, 247, No. 012007.
- (63) Frisch, M. J., et al., Gaussian 16, Revision C.01, Gaussian, Inc., Wallingford CT, 2016.
- (64) Wolfe, J. F.; Loo, B. H.; Arnold, F. E. Rigid-Rod Polymers. 2. Synthesis and Thermal Properties of Para-Aromatic Polymers with 2,6-Benzobisthiazole Units in the Main Chain. *Macromolecules* **1981**, 14, 915–920.
- (65) Roberts, M. F.; Jenekhe, S. A. Lewis-Acid Coordination-Complexes of Polymers. 3. Poly(Benzimidazobenzophenanthroline) Ladder and Semiladder Polymers. *Polymer* **1994**, *35*, 4313–4325.
- (66) Lee, B. H.; Marvel, C. S. Rigid-Ladder Polymers: Polymers Containing Anthraquinone Recurring Units. *J. Polym. Sci., Part A: Polym. Chem.* **1983**, 21, 83–87.
- (67) Antonidas, H.; Abkowitz, M. A.; Osaheni, J. A.; Jenekhe, S. A.; Stolka, M. Effects of Humidity on the Dark Conductivity and Dielectric-Properties of Poly(Benzimidazobenzophenanthroline) Thin-Films. *Chem. Mater.* **1994**, *6*, 63–66.
- (68) Choudhury, S. D.; Basu, S. Interaction of Phenazine with Water and DNA Bases. *Spectrochim. Acta, Part A* **2005**, *62*, 736–739.
- (69) Lee, J.; Kalin, A. J.; Yuan, T.; Al-Hashimi, M.; Fang, L. Fully Conjugated Ladder Polymers. *Chem. Sci.* **2017**, *8*, 2503–2521.
- (70) Fazzi, D.; Negri, F. Addressing the Elusive Polaronic Nature of Multiple Redox States in a π -Conjugated Ladder-Type Polymer. *Adv. Electron. Mater.* **2021**, 7, 2000786.
- (71) Onwubiko, A.; Yue, W.; Jellett, C.; Xiao, M.; Chen, H.-Y.; Ravva, M. K.; Hanifi, D. A.; Knall, A.-C.; Purushothaman, B.; Nikolka, M.; Flores, J.-C.; Salleo, A.; Brédas, J. L.; Sirringhaus, H.; Hayoz, P.; McCulloch, I. Fused Electron Deficient Semiconducting Polymers for Air Stable Electron Transport. *Nat. Commun.* **2018**, *9*, 416.
- (72) Fazzi, D.; Fabiano, S.; Ruoko, T. P.; Meerholz, K.; Negri, F. Polarons in Pi-Conjugated Ladder-Type Polymers: A Broken Symmetry Density Functional Description. *J. Mater. Chem. C* **2019**, 7, 12876–12885.
- (73) Brédas, J. L.; Beljonne, D.; Coropceanu, V.; Cornil, J. Charge-Transfer and Energy-Transfer Processes in π-Conjugated Oligomers and Polymers: A Molecular Picture. *Chem. Rev.* **2004**, *104*, 4971–5004.
- (74) Zade, S. S.; Zamoshchik, N.; Bendikov, M. From Short Conjugated Oligomers to Conjugated Polymers. Lessons from Studies on Long Conjugated Oligomers. *Acc. Chem. Res.* **2011**, *44*, 14–24.
- (75) Quinto, M.; Jenekhe, S. A.; Bard, A. J. Polymer Films on Electrodes. 30. Electrochemistry and Scanning Electrochemical Microscopy Characterization of Benzimidazolebenzophenanthroline-

- Type Ladder (BBL) and Semiladder (BBB) Polymer Films. Chem. Mater. 2001, 13, 2824–2832.
- (76) Jenekhe, S. A.; Lu, L.; Alam, M. M. New Conjugated Polymers with Donor–Acceptor Architectures: Synthesis and Photophysics of Carbazole–Quinoline and Phenothiazine–Quinoline Copolymers and Oligomers Exhibiting Large Intramolecular Charge Transfer. *Macromolecules* **2001**, *34*, 7315–7324.
- (77) Agrawal, A. K.; Jenekhe, S. A. Synthesis and Processing of Heterocyclic Polymers as Electronic, Optoelectronic, and Nonlinear Optical Materials. 2. New Series of Conjugated Rigid-Rod Polyquinolines and Polyanthrazolines. *Macromolecules* 1993, 26, 895–905.
- (78) Spano, F. C.; Silva, C. H- and J-Aggregate Behavior in Polymeric Semiconductors. *Annu. Rev. Phys. Chem.* **2014**, *65*, 477–500.
- (79) Más-Montoya, M.; Janssen, R. A. J. The Effect of H- and J-Aggregation on the Photophysical and Photovoltaic Properties of Small Thiophene–Pyridine—DPP Molecules for Bulk-Heterojunction Solar Cells. *Adv. Funct. Mater.* **2017**, *27*, 1605779.
- (80) Pschirer, N. G.; Bunz, U. H. F. Poly(Fluorenyleneethynylene)s by Alkyne Metathesis: Optical Properties and Aggregation. *Macromolecules* **2000**, *33*, 3961–3963.
- (81) Kim, F. S.; Hwang, D. K.; Kippelen, B.; Jenekhe, S. A. Enhanced Carrier Mobility and Electrical Stability of N-Channel Polymer Thin Film Transistors by Use of Low-k Dielectric Buffer Layer. *Appl. Phys. Lett.* **2011**, *99*, 173303.
- (82) An, X.; Wang, K.; Bai, L.; Wei, C.; Xu, M.; Yu, M.; Han, Y.; Sun, N.; Sun, L.; Lin, J.; Ding, X.; Xie, L.; Zhang, Q.; Qin, T.; Huang, W. Intrinsic Mechanical Properties of the Polymeric Semiconductors. *J. Mater. Chem. C* **2020**, *8*, 11631–11637.
- (83) Zheng, Y.; Wang, G. J. N.; Kang, J.; Nikolka, M.; Wu, H. C.; Tran, H.; Zhang, S.; Yan, H.; Chen, H.; Yuen, P. Y.; Mun, J.; Dauskardt, R. H.; McCulloch, I.; Tok, J. B. H.; Gu, X.; Bao, Z. An Intrinsically Stretchable High-Performance Polymer Semiconductor with Low Crystallinity. *Adv. Funct. Mater.* **2019**, 29, 1905340.
- (84) Root, S. E.; Savagatrup, S.; Printz, A. D.; Rodriquez, D.; Lipomi, D. J. Mechanical Properties of Organic Semiconductors for Stretchable, Highly Flexible, and Mechanically Robust Electronics. *Chem. Rev.* **2017**, *117*, 6467–6499.
- (85) Zhang, S.; Galuska, L. A.; Gu, X. Water-Assisted Mechanical Testing of Polymeric Thin-Films. *J. Polym. Sci.* **2021**, *60*, 1108–1129.
- (86) Chen, A. X.; Kleinschmidt, A. T.; Choudhary, K.; Lipomi, D. J. Beyond Stretchability: Strength, Toughness, and Elastic Range in Semiconducting Polymers. *Chem. Mater.* **2020**, *32*, 7582–7601.
- (87) Xiao, M.; Sadhanala, A.; Abdi-Jalebi, M.; Thomas, T. H.; Ren, X.; Zhang, T.; Chen, H.; Carey, R. L.; Wang, Q.; Senanayak, S. P.; Jellett, C.; Onwubiko, A.; Moser, M.; Liao, H.; Yue, W.; McCulloch, I.; Nikolka, M.; Sirringhaus, H. Linking Glass-Transition Behavior to Photophysical and Charge Transport Properties of High-Mobility Conjugated Polymers. *Adv. Funct. Mater.* **2021**, *31*, 2007359.
- (88) Zhang, Z.; Yu, Y.; Tang, Y.; Guan, Y.; Hu, Y.; Yin, J.; Willets, K.; Ren, S. Kirigami-Inspired Stretchable Conjugated Electronics. *Adv. Electron. Mater.* **2020**, *6*, 1900929.
- (89) Powell, J. W.; Chartoff, R. P. Viscoelastic properties and stability of BBL ladder polymers. *J. Appl. Polym. Sci.* **1974**, *18*, 83–91.
- (90) Wang, C. S.; Lee, C. Y. C.; Arnold, F. E. Mechanical and Electrical Properties of Heat-Treated Ladder Polymer Fiber. MRS Proc. 1992, 247, 747.
- (91) Giridharagopal, R.; Flagg, L. Q.; Harrison, J. S.; Ziffer, M. E.; Onorato, J. W.; Luscombe, C. K.; Ginger, D. S. Electrochemical Strain Microscopy Probes Morphology-Induced Variations in Ion Uptake and Performance in Organic Electrochemical Transistors. *Nat. Mater.* **2017**, *16*, 737–742.
- (92) Flagg, L. Q.; Bischak, C. G.; Onorato, J. W.; Rashid, R. B.; Luscombe, C. K.; Ginger, D. S. Polymer Crystallinity Controls Water Uptake in Glycol Side-Chain Polymer Organic Electrochemical Transistors. *J. Am. Chem. Soc.* **2019**, *141*, 4345–4354.